AIAA JOURNAL
Vol. 46, No. 1, January 2008

Variable Structure Model for Flow-Induced Tonal Noise Control with Plasma Actuators

Xun Huang,* Sammie Chan,† Xin Zhang,‡ and Steve Gabriel§
School of Engineering Sciences, University of Southampton, Southampton, SO17 1BJ, United Kingdom

DOI: 10.2514/1.30852

The objective of this work was to study the effect of plasma actuators in attenuating low-speed flow-induced cavity tones from a control point of view by employing techniques from classical control. A modification of the existing physics-based linear model produced a new variable structure model in which a plasma actuator was regarded as a linear gain. The parameters of the overall model working at two operating voltages were identified using experimental data. The effects of the plasma actuator control at other various operating voltages were thus able to be predicted using linear interpolation. The good agreement between the predicted and the measured data supported the proposed variable structure model, inside of which plasma actuators affected the damping of cavity pressure oscillations proportionally to the applied voltage to reduce flow-induced tonal noise. With the proposed variable structure model the system stability controlled by plasma actuators at various operating voltages was ensured, thus a closed-loop control method could be applied without leading to instability. A simple proportional integral derivative controller was implemented. Results show the potential of a closed-loop method by increasing system power efficiency.

Nomenclature

$Ac(s)$	=	transfer function of an actuator
$A(s)$	=	transfer function of acoustic feedback
$C(s)$	=	transfer function of a controller
C_p	=	mean phase speed
c_0	=	speed of sound
$G(s)$	=	transfer function of shear layer
f_p	=	dominant Rossiter frequency
K_r	=	receptivity constant
K_s	=	scattering constant
L	=	cavity length
M	=	freestream Mach number, U_∞/c_0
n	=	Rossiter mode number
$Pm(s)$	=	transfer function of plasma actuators
$P(s)$	=	transfer function of overall plant model
r_a	=	constant parameter in acoustic delay part
St	=	Strouhal number, f_pL/U_∞
s	=	complex parameter for Laplace transform
U_∞	=	freestream velocity
V_{DC}	=	direct current voltage of the system power supply
V_{dz}	=	dead-zone voltage
V_{pp}	=	peak-to-peak voltage
x, y, z	=	Cartesian coordinates
γ	=	the phase shift in the Rossiter's formula
δ	=	boundary-layer thickness
κ	=	a variable in the Rossiter's formula, C_p/U_∞
ξ	=	damping ratio of a second-order system
τ_a	=	acoustic propagation delay
τ_s	=	fluid convection time
ω_p	=	dominant Rossiter angular frequency, $2\pi f_p$
ω_r	=	constant parameter in acoustic delay part
ω_0	=	natural angular frequency of a second-order system

Presented as Paper 2007-3561 at the 13th AIAA/CEAS Aeroacoustics Conference, Rome, Italy, 21–23 May 2007. Received 6 March 2007; revision received 14 October 2007; accepted for publication 14 October 2007.

*University Fellow, Aeronautics and Astronautics; xunger@soton.ac.uk. AIAA Member.

†Research Fellow, Aeronautics and Astronautics; sccchan@soton.ac.uk. AIAA Member.

‡Professor, Aeronautics and Astronautics; x.zhang1@soton.ac.uk. Associated Fellow AIAA.

§Professor, Aeronautics and Astronautics; sbg2@soton.ac.uk. AIAA Member.

I. Introduction

PLASMA, operating in atmospheric pressure air, can induce fluid motion to the surrounding neutral gas that can serve flow control applications [1–11]. Several types of atmospheric pressure glow discharge plasma actuators have been developed and used for flow control applications, two of which are one atmosphere uniform glow discharge plasma (OAUGDP) actuators [1–5] and dielectric barrier discharge actuators [6–8]. The fundamental structure of the plasma actuator used in this study is similar to an OAUGDP actuator that is able to generate weakly ionized atmospheric plasma, which couples the neutral fluid to an electric field. Through Lorentzian collisions, momentum is transferred to the neutral gas via charged particles in nitrogen/oxygen plasma, thus affecting the flowfield local to the plasma actuator [3].

More recently, plasma actuator technology has been applied to aeroacoustic applications [12–14]. The principle of using plasma actuators for aeroacoustic noise control is to sufficiently modify the flowfield to disrupt or minimize the mechanisms of flow-induced noise. Our previous work [13,14] demonstrated the use of plasma actuators for attenuating cavity tonal noise that is similar to landing gear bay noise. The problem has been frequently employed as a testbed in the study of flow-induced noise control [15–18]. The simplicity and absence of any mechanical moving parts, for example, pumps, make the plasma actuator a promising option for aeroacoustic applications. To improve efficiency, the plasma actuator has been integrated into a closed-loop control system, using the cavity as a test case again. It is therefore necessary to develop a linear [19]/nonlinear [20] model of the cavity system under control [21] with plasma actuators, by which the fundamental properties, for example, stability, of the proposed closed-loop control method can be assessed. Control methodologies for a linear model are already well developed in the control system society. To apply the linear control analysis and design techniques, a linear model is generally preferred. For instance, a linearly approximated model, instead of the

nonlinear state-space model originally presented in the literature [20], was used to design a linear quadratic regulator [20].

Several linear models developed for closed-loop control applied to cavity flow-induced tonal noise exist [17,19,22]. An empirical model developed by Cattafesta et al. using adaptive system identification cooperated with a disturbance rejection algorithm to suppress cavity pressure fluctuations [17]. To obtain the frequency response of an empirical model, the ideal input has a flat spectral density. The plasma actuator, however, works efficiently between a narrow range of radio frequencies so that it is not straightforward to operate system identification over a dynamic process controlled with plasma actuators. The physics-based linear model developed by Rowley et al. approximated the dynamics of the shear layer using linear stability theory and regarded acoustic scattering and the receptivity of the shear layer as constant gains [19]. Based on this analytical model, several classical control techniques, such as root locus and Bode and Nyquist plots, have been applied to analyze the cavity dynamics affected by a potential closed-loop control strategy [19].

The main objective of this study is to demonstrate that by modifying the physics-based linear model of Rowley et al. [19] by considering the plasma actuator as a linear gain, one can explain the effect of plasma actuators for the suppression of flow-induced cavity tones from a control point of view. A feedback system was subsequently developed to demonstrate the potential of closed-loop control methods using plasma actuators. The paper is organized as follows. Section II reviews the existing open-loop system controlled with a plasma actuator. Section III introduces an existing physics-based linear model, for which a new variable structure model is developed to include the effect of the plasma actuator (Sec. IV). A proportional integral derivative (PID) controller is used to demonstrate the closed-loop system in Sec. V. Finally, Sec. VI summarizes the present model and results.

II. Open-Loop Control with a Plasma Actuator

To generate atmospheric glow discharge plasma in air, a sufficiently high potential is required to breakdown the surrounding species [23]. As displayed in Fig. 1, the potential is applied at a plasma driving frequency of several kilohertz (kHz) to sustain the glow discharges and to prevent electron avalanches that lead to arcing [23]. In this study, a square wave of the plasma driving frequency with an adjustable duty cycle generated by a pulse width modulation (PWM) module of a dSPACE real-time system is fed into a metal-oxide-semiconductor field-effect transistor (MOSFET) driver. The driver provides current to the gate of a power MOSFET, thus reducing the switching power losses of the power MOSFET. The source of the power MOSFET is grounded and the drain of the power MOSFET is connected to a step-up transformer. As the power MOSFET is switched on/off by the plasma driving signal, the transformer generates the high-voltage output sufficient to induce the discharges. Generally, a bigger duty cycle of the PWM driving signal corresponds to a stronger magnetic field created on the magnetic coil and subsequently a higher voltage output. The performance of the plasma actuator is therefore controlled by adjusting the duty cycle of the PWM driving signal.

The plasma actuator is composed of a series of symmetrical electrodes that are manufactured to be aligned with the oncoming flow. The cathodes (grounded electrodes) are wider than the anodes that are located on the upper flow facing surface (Fig. 1). After applying high voltages, from the narrow anodes to the wide cathode there is subsequently an electric field leading to air discharges mainly happening in the flow facing surface. The actuator with symmetric geometries therefore induces fluid motion along the surface of the dielectric board leading to the formation of streamwise vortical structures, between a pair of actuators, that are transported downstream with the flow, introducing three-dimensional effects across the span of the cavity. It is also worth noting that with a reversed geometry, that is, the anodes are wider than the cathodes, the major discharges will unfavorably happen in the bottom surface and thus are useless to manipulate flow local to the upper surface. In addition, with asymmetric geometry [24], an induced fluid velocity

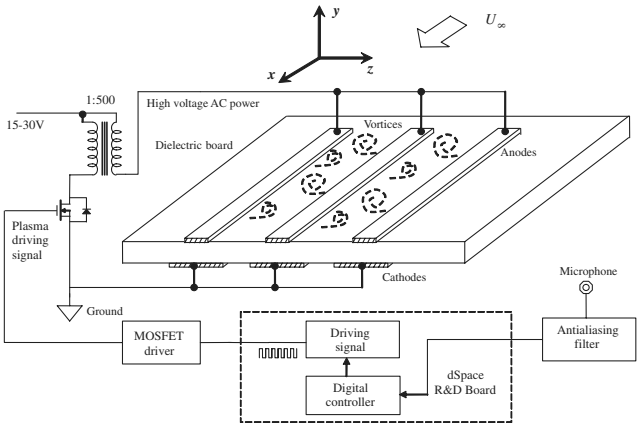

Fig. 1 The symmetrical structure of a plasma actuator used in wind-tunnel experiments.

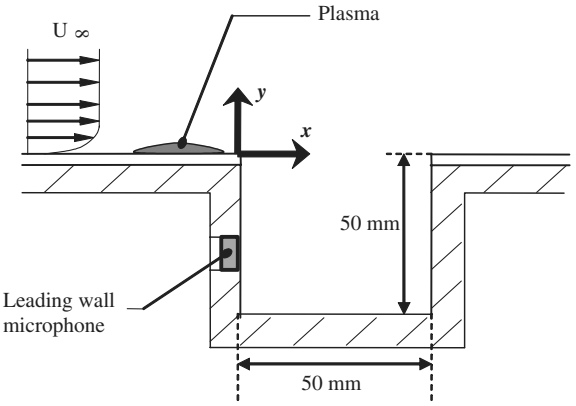

Fig. 2 The cavity model setup with a plasma actuator and a sound pressure sensor.

up to 8 m/s was discovered in our lab near the surface of the dielectric plate. It also attenuated flow-induced noise but with a different mechanism that is beyond the scope of this paper.

Experiments were conducted in a wind-tunnel facility at the University of Southampton. The wind tunnel is of a closed jet, open-loop design. The maximum flow speed attainable in the working section of the tunnel is 25 m/s. The working section has a uniform cross section that measures 0.260×0.345 m and has a length of 0.850 m. A cavity model (Fig. 2) manufactured from Perspex is used as a testbed to develop the plasma actuator control system. A leading-edge plate upstream of the cavity, 150 mm long, provides a boundary-layer thickness of $\delta = 6.1$ mm at 10 m/s. The leading-edge plate was made from printed circuit board, allowing the plasma actuator to be etched into the leading-edge plate. The investigation was performed for the cavity with a geometry length-to-depth ratio of 1.0 at flow speeds ranging from 10 to 20 m/s, corresponding to Reynolds numbers of 3.6×10^4 and 7.2×10^4 respectively.

Surface pressure measurements of the cavity were recorded using a Panasonic WM-60A omnidirectional condenser microphone that was flush mounted to the surface of the cavity's front wall. The installation distance to the leading-edge plate is 25 mm. The microphone's signal was passed through an antialiasing filter and then sampled with a personal computer sound card and an analog-to-digital converter (ADC) of the dSPACE real-time system. For the closed-loop control system, the dSPACE system sampled the microphone signal at 10 kHz. For the frequency spectrum presented in this paper, the personal computer sound card sampled the microphone signal at 44.1 kHz.

The performance of the open-loop control system at attenuating the flow-induced cavity tones is shown in Fig. 3 [13]. A 4096-point fast Fourier transform with a Hanning window function is applied to the sampled data. The sound pressure level (SPL) result is averaged

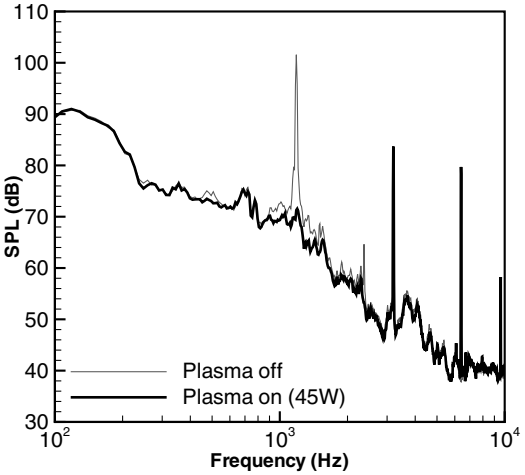

Fig. 3 Open-loop control with a plasma actuator attenuating cavity tonal noise. The freestream velocity $U_\infty = 20$ m/s.

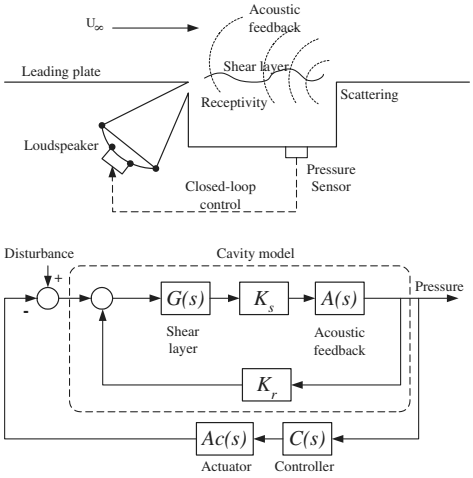

Fig. 4 Closed-loop control with the schematic of the physics-based linear model [19].

over 300 signal blocks for statistical confidence. The frequency spectrum in Fig. 3 shows the tonal noise is attenuated to broadband levels with the system operating at 30 volts (V) and using 45 watts (W). The driving signal of the plasma actuator is a 3.2 kHz square wave with a 50% duty cycle. Other than attenuating flow-induced tonal noise, the plasma actuator also radiates high-frequency tones that are harmonics of the plasma driving signal. The experimental data [13] show that the amplitude of the high-frequency tones increases along with the input power. More details related to the physics of glow discharges affecting the fluid dynamics and acoustics have been given in the previous work [13,14] and will not be repeated here. To improve the power efficiency for potentially large plasma actuators, a closed-loop control system is believed to reduce power consumption compared with an open-loop system [25]. Before the design of a closed-loop control method, however, it is important to have an analytical model describing the system dynamics under control by the plasma actuator so that the fundamental properties of the proposed control method can be assessed.

III. Physics-Based Linear Model

Several closed-loop control methodologies, such as optimal control [15], adaptive control [26], and robust control [16], that use linear models have been applied successfully in attenuating flow-induced cavity tones. The linear models in the former two designs were constructed using system identification techniques. The third design was based on a physics-based linear model that was presented by Rowley et al. [19]. The physics-based model is heuristic for our work. It is introduced briefly below. A simple closed-loop system schematic with the physics-based model is displayed in Fig. 4. The definitions of the parameters in Fig. 4 are given in the next paragraph. The disturbances in the boundary layer on the leading-edge plate are considered, whereas measurement noises are not. The disturbances in the boundary layer are amplified and propagated by the shear layer to the trailing edge, where sound is generated and scattered back to the leading edge, which feeds back into the shear layer and thus adds disturbances to the system. Several pressure sensors were mounted on the front wall, the rear wall, and the bottom floor to measure the instantaneous pressure signal [19]. For simplicity, only one pressure sensor is displayed in Fig. 4. A specifically designed controller drives the actuator to reduce the pressure oscillations [19,20,25]. A loudspeaker was employed as the actuator in the literature [19]. Other actuators like piezoelectric actuators and oscillating flaps were also investigated [20,22]. A thorough review of various actuators (excluding plasma actuators) with open-loop and closed-loop control methods can be found in Rowley et al. [22] and Cattafesta et al. [25].

More precisely, the linear model presented by Rowley et al. [19] is capable of predicting cavity dynamics using several linear transfer functions: the shear layer dynamics $[G(s)]$; the acoustic feedback $[A(s)]$; scattering gain (K_s) at the trailing edge; and the receptivity gain (K_r) at the leading edge of a cavity, where s is a complex parameter associated with the Laplace transform, and K_r and K_s are assumed to be constants [16,19]. The function $A(s)$ is a part of the acoustic propagation delay from the trailing-edge corner to the leading-edge corner of a cavity [16]:

$$A(s) = \frac{e^{-\tau_a s}}{1 - r(s)e^{-2\tau_a s}}, \qquad r(s) = \frac{r_a}{1 + s/\omega_r} \tag{1}$$

τ_a is the acoustic propagation delay, and ω_r and r_a are constants [16]. The function $G(s)$ is a second-order system [27] that includes fluid convection time delay [19]:

$$G(s) = \frac{\omega_0^2 e^{-\tau_s s}}{s^2 + 2\xi\omega_0 s + \omega_0^2} \tag{2}$$

The natural angular frequency ω_0 and the damping ratio ξ are related to the frequency and the amplitude of the dominant Rossiter mode [28]. The variable τ_s is the fluid convection time: $\tau_s = L/C_p$ [19], where L is the cavity length from the leading-edge corner to the trailing-edge corner; C_p is the mean phase speed, $C_p/U_\infty = \kappa$, where $\kappa = 0.625$ [28]; and $U_\infty = Mc_0$, where M is the freestream Mach number and c_0 is the speed of sound. The parameter values for one example can be found in Table 1. The overall cavity plant model $P(s)$ is:

Table 1 The parameter values of the system model, where $U_\infty = 20$ m/s, and r_a, ω_r, K_r, and K_s were given in the literature [16]: $r_a = 0.01$, $\omega_r = 20000$ rad/s, $K_r = 0.01$, $K_s = 5.0$

Parameter	Actuator inactive	Actuator working at 16 V, 13 W	Actuator working at 30 V, 45 W
ω_p	7194.2 rad/s	7194.2 rad/s	7194.2 rad/s
ω_0	7197.1 rad/s	7262.4 rad/s	8724.3 rad/s
ξ	0.02	0.097	0.4
τ_s	0.0017 s	0.0017 s	0.0017 s
τ_a	0.00015 s	0.00015 s	0.00015 s

$$P(s) = \frac{G(s)A(s)K_s}{1 \pm G(s)A(s)K_sK_r} \tag{3}$$

where the sign $\pm$ denotes that both positive and negative feedbacks may appear in the cavity system. A more detailed discussion on the derivation of the physics-based linear model and the associated physical meaning of the given parameters can be found in Rowley et al. [19].

IV. Variable Structure Model

Several issues prevent us from employing the physics-based linear model directly with plasma actuators. In our previous experiments with the open-loop control scheme [13], measurements with particle imaging velocimetry (PIV) demonstrated that cavity resonance was minimized by using plasma actuators to produce a spanwise variation of the flow through induced vortices rather than providing streamwise perturbations. Three-dimensional disturbances introduced into the cavity's shear layer impeded the development of organized structures in the cavity shear layer, thus disrupting the feedback mechanism that was to sustain the fluid-acoustic process. The attenuation of cavity oscillations by changing the three-dimensional flowfield resembles a variable structure process rather than a time invariant process. Figure 5 shows a potential closed-loop scheme with the tentative variable structure. The physics-based linear model is still employed while the inner shear layer model is variable with the plasma actuator, whose model is to be studied next from a control point of view.

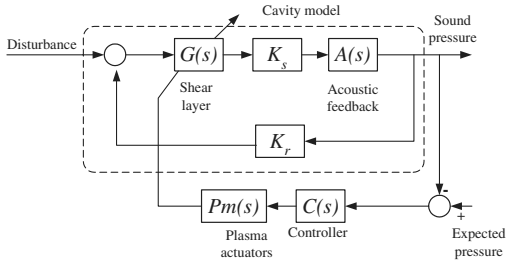

Fig. 5 Closed-loop control with the variable structure model using plasma actuators.

Several endeavors have been presented to model plasma actuators through plasma physics [29], fluid physics [30], and electronic circuit representation [31]. The former two efforts computationally explored the interaction between plasma discharges and the surrounding flow using particle-in-cell direct simulation, the Monte Carlo method, and Navier–Stokes equations, which reflect the highly nonlinear physics that are hardly to be contained in a linear control system. The third effort set up a lump circuit model to simulate electric properties of the plasma discharge and the associated driving circuits using PSPICE, a commercial version of simulation program with integrated circuit emphasis (SPICE). The method is helpful to optimize the driving circuit, although it provides little insight into the interaction between flow and discharges.

In this work, the effect of a plasma actuator on attenuating flow-induced cavity tone will be studied with several analysis tools, such as phase portrait and parameter identification, available in the

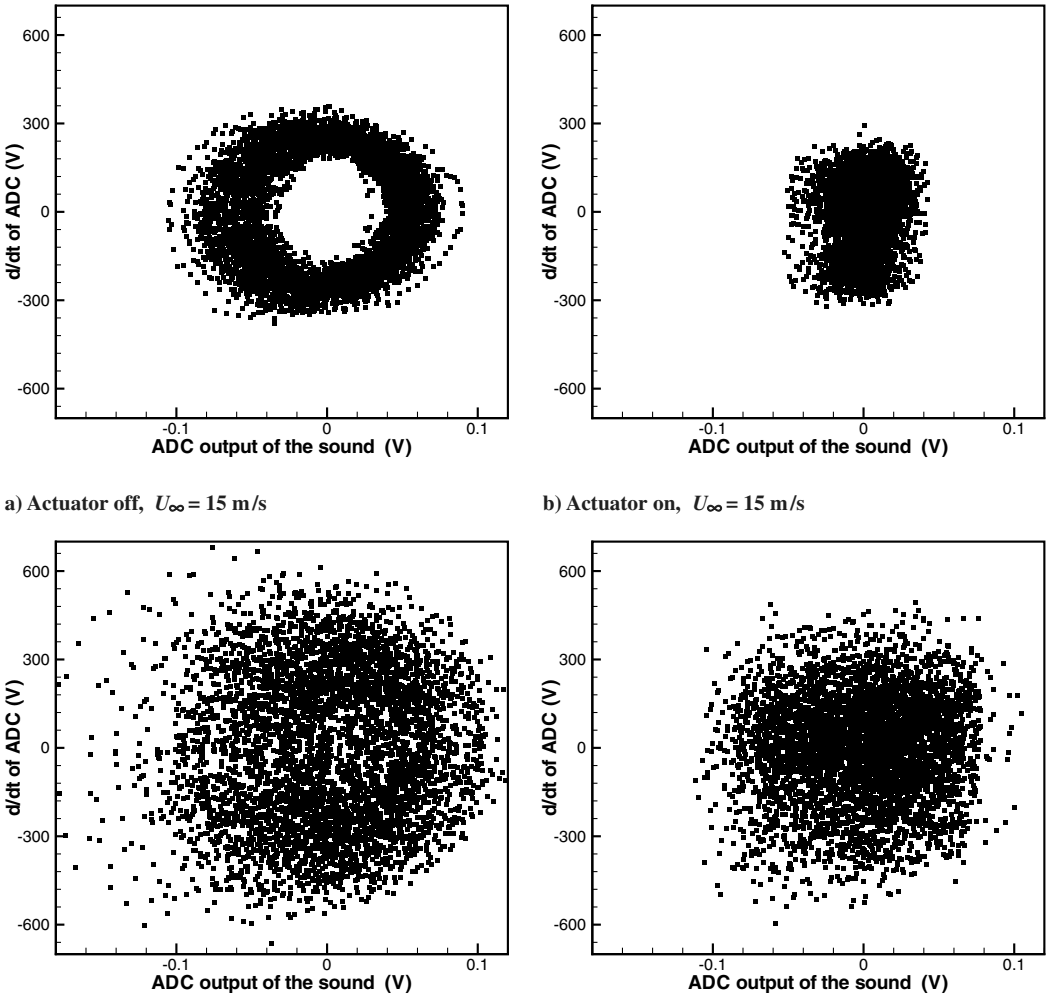

a) Actuator off, $U_\infty = 15$ m/s **b) Actuator on, $U_\infty = 15$ m/s**

c) Actuator off, $U_\infty = 20$ m/s **d) Actuator on, $U_\infty = 20$ m/s**

Fig. 6 Phase portraits of the surface pressure signals sampled from the leading-edge microphone.

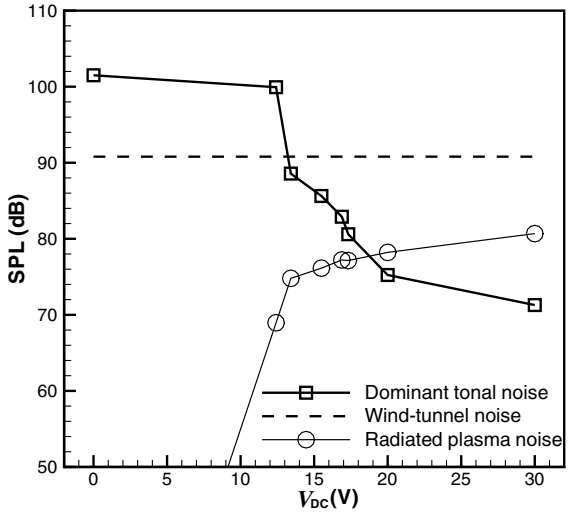

Fig. 7 Amplitudes of the attenuated dominant tonal noise (1186 Hz) and the radiated plasma noise (3200 Hz) against the system input low DC voltages.

classical control theory. A phase portrait is normally used in nonlinear control to analyze system dynamics in a two-dimensional phase plane. The technique was used by Rowley et al. [19] to study the stability of the flow-induced sound oscillation in a cavity. Figure 6 shows several phase portraits of the sound pressure data collected from an ADC of the dSPACE real-time system at two different freestream velocities. The microphone is installed on the front wall of the cavity (Fig. 2). At $U_\infty = 15$ m/s with no plasma actuation, the phase portrait can be characterized as a limit cycle, indicating that the system might be unstable and that nonlinear viscous effects saturate the pressure oscillations. At $U_\infty = 20$ m/s with no plasma actuation, the phase portrait is focused around a central point, which implies that the system is stable. Figure 6 also shows that the plasma actuator stabilizes the unstable system at $U_\infty = 15$ m/s and reduces the sound pressure amplitudes for both cases at $U_\infty = 15$ and 20 m/s. A transfer function can be estimated as long as the corresponding system is stable; the frequency spectrum at $U_\infty = 20$ m/s was therefore used to study the system transfer functions with/without plasma actuation, through which the effect of plasma actuators can be deduced.

Figure 3 shows that the cavity tonal noise was attenuated to broadband level when the plasma actuator was supplied with 30 V and 45 W of system power. Furthermore, Fig. 7 compares the dominant tonal noise and the radiated plasma noise related to different input DC voltages (V_{DC}) . The corresponding peak-to-peak high-output AC voltage (V_{pp}) of the transformer is from 0 to 15 kilovolts (kV). Figure 7 shows that the effect of attenuation increases along with the applied voltage while the undesirable by-product, plasma noise radiation, is also increased. To determine the relationship between the plasma actuator and its attenuation effect, two important equations of the second-order linear system with fluid convection time delay, which are well known in classical control [27], are used:

$$\omega_p = \omega_0\sqrt{1-2\xi^2}, \qquad |G(j\omega)|_{\omega=\omega_p} = \frac{\omega_0}{2\xi\omega_p} \tag{4}$$

where ω_p is the dominant Rossiter angular frequency and $j\omega = s$. As mentioned earlier, the ideal input disturbance has a flat power spectrum; the spectrum of the system output is proportional to the magnitude of the system transfer function $P(s)$, which is found to be mainly dependant on the shear layer model $G(s)$ [16]. According to Eq. (4), we have

$$\text{SPL} \propto |G(s)| \propto \frac{1}{2\xi\sqrt{1-2\xi^2}} \tag{5}$$

For a small ξ ($\xi \ll 1$), SPL is approximately proportional to $1/\xi$. Meanwhile, from Fig. 7 it can be seen that the relationship between SPL and system voltage V_{DC} approximately satisfies SPL $\propto 1/V_{DC}$ (when $V_{DC} > 12$ V). After comparing the expression in Eq. (5) with the graphic in Fig. 7, the relation between V_{DC} and ξ is therefore approximately linear. Effectively, the damping ratio (ξ) of the cavity system can be controlled by a plasma actuator through proportional adjustment of V_{DC}, in this work, which has been implemented using the PWM circuits. Figure 7 also shows that when the system input voltage $V_{DC} \le 12$ V, the output voltage (with $V_{pp} \le 9$ kV) generates quite weak discharges. The plasma actuator has little effect on the flow-induced tonal noise. For our model, this voltage range is described by a dead zone.

As the effect of a plasma actuator has been regarded as a linear gain, the system performance with plasma actuation can be predicted when the parameter values at any two operating voltages are identified. Table 1 lists the parameter values of the system at $V_{DC} =$ 0 and 30 V that were identified according to Eqs. (2–4). In our numerical experiments, it was found that the shape of the SPL results mainly depends on $G(s)$. The values of ω_r, K_r, and K_s given in the literature [16] also work for our test case. The acoustic propagation delay τ_a depends only on the sound speed. The fluid convection time τ_s depends on the dominant Rossiter frequency f_p. Recall that the Rossiter's empirical formula [28] is

$$St = \frac{f_p L}{U_\infty} = \frac{n-\gamma}{M+\frac{1}{\kappa}} \tag{6}$$

where St is the Strouhal number, n is the Rossiter mode number, γ is the phase shift that is an empirically selected constant, and $\kappa = C_p/U_\infty$ and $\tau_s = L/C_p$. In our experiments with the plasma actuation f_p ($f_p = \omega_p/2\pi$) was fixed, although the amplitude of the sound pressure at f_p was attenuated. The constant f_p suggests that κ is not affected by the plasma actuation. Therefore, both τ_s and τ_a are constants in Table 1.

The system performance at $U_\infty = 20$ m/s controlled by the plasma actuator applied with other input voltages can thereafter be predicted by the following linear interpolation equation:

$$\xi(V_{DC}) = \xi|_{V_{DC}=0} + (\xi|_{V_{DC}=30} - \xi|_{V_{DC}=0}) \times (V_{DC} - V_{dz})/(30 - V_{dz}), \qquad (V_{DC} > V_{dz}) \tag{7}$$

where V_{dz} models the dead zone, V_{dz} is 12 V according to Fig. 7, and $\xi(V_{DC}) = \xi|_{V_{DC}=0}$ if $V_{DC} \le V_{dz}$. For example, the corresponding parameters when $V_{DC} = 16$ V are computed and listed in Table 1.

The modeled and the measured data at two operating voltages (0 and 30 V) are compared in Figs. 8a and 8b. It is shown that both the modeled and the measured data drop 40 dB/decade after the dominant Rossiter frequency. There is a less than 3 dB difference at the maximum amplitude between the modeled and the measured SPL data. Both the wind-tunnel background noise and the plasma noise are not considered in the model. Therefore, there is an approximately 20 dB difference in the low-frequency part that is dominated by the wind-tunnel background noise. The harmonics of the radiated plasma noise also do not appear in the modeled results. With the parameter values ($\xi|_{V_{DC}=0}$ and $\xi|_{V_{DC}=30}$) obtained in the modeling procedures of Figs. 8a and 8b, the SPL results at other voltages can be predicted by using Eq. (7). As an example, Fig. 8c shows a prediction result of the system applied with a 16 V system input voltage. The corresponding parameter values are already listed in Table 1. In addition, compared with the empirical solutions in Table 2, the SPL results in Fig. 8c show that the energy of the dominant mode (the fifth mode) is attenuated and redistributed to the other mode (the fourth mode) with a smaller energy level. The similar phenomenon for feedback control methods was reported by Samimy et al. [20]. There is still a feedback loop between the external disturbances and the output sound pressure level, even if the closed-loop controller $C(s)$ does not exist for an open-loop plasma control system.

The peak amplitudes of the dominant tonal noise associated with V_{DC} are predicted using Eqs. (2–5) and (7) and compared with the

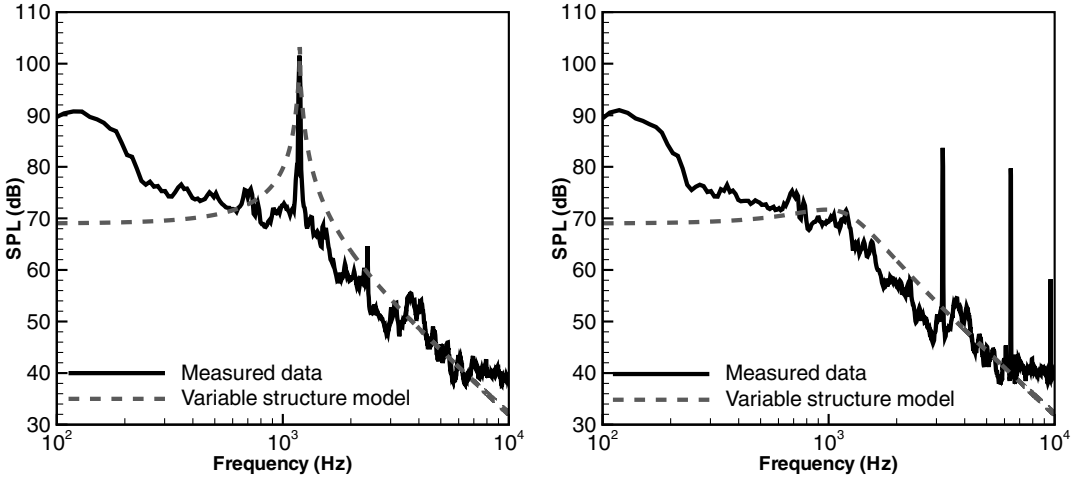

a) Actuator off

b) Actuator on, V_{DC} = 30V, system power 45 W

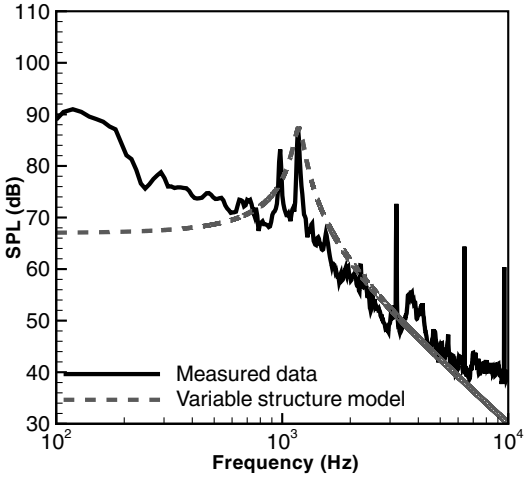

c) Actuator on, V_{DC} = 16V, system power 13.5 W

Fig. 8 The measured and modeled SPL results at $U_\infty = 20$ m/s.

measured data in Fig. 9. The predictions are shown to match the measured data quite well. It confirms the assertion that, from the perspective of control, the damping ratio of a cavity system is controlled by the plasma actuator proportionally to the supplied input voltage V_{DC}.

Time delays in the cavity model were approximated with Padé approximation [32], which shows that a time delay increases the system model order and produces a cluster of open-loop system zeros on the right half of the complex plane that might pull closed-loop system poles into the right half of the complex plane and break the system stability when an improper feedback gain is used. With the variable structure model, we can study the stability of a closed-loop control system with the plasma actuator. The root locus technique commonly used in classical control that could give closed-loop pole trajectories as a function of the feedback gain is not applicable to the variable structure model. The locus of the poles and zeros of the model related to V_{DC} from 0 to 30 V is therefore directly computed with Eqs. (2–5) and (7), in which the voltage interval used in the prediction equation [Eq. (7)] is 0.1 V. Results are displayed in Fig. 10, which shows that the closed-loop system poles are all located on the left half of the complex plane. As the model is linear, Fig. 10 guarantees the stability of a potential closed-loop system using the plasma actuator.

Rather than employing the variable structure model, the increase of the pressure oscillation damping using the plasma actuator is analogous to a velocity feedback in electric motor control applications. It implies that a differential part might exist between the cavity pressure output and the shear layer disturbance input, according to the present results, whose gain is attenuated with the plasma actuator proportionally to the applied voltage. In that case the classical feedback control structure, as displayed in Fig. 4, can be employed to design and analyze a control method. However, at the moment it is difficult to prove with physics that a differential part caused by glow discharges does exist. The exact physics calls for further studies. The present variable structure model is intuitional and straightforward. The model is helpful to explain the working mechanisms of plasma actuators.

V. Closed-Loop Control with a Plasma Actuator

As the closed-loop system is stable with various input voltages, a simple feedback control strategy can be applied to improve the power

Table 2 The dominant frequencies predicted by the Rossiter formula [28]

Velocities and modes	First mode	Second mode	Third mode	Fourth mode	Fifth mode	Sixth mode
15 m/s	137 Hz	319 Hz	502 Hz	684 Hz	866 Hz	1049 Hz
20 m/s	181 Hz	422 Hz	663 Hz	904 Hz	1145 Hz	1387 Hz

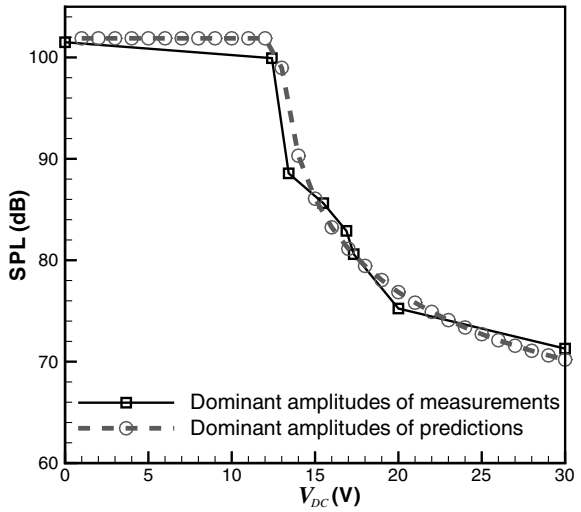

Fig. 9 Dominant amplitudes of the measured and the predicted tonal noise against the input low DC voltages at $U_\infty = 20$ m/s.

efficiency: V_{DC} applied to the plasma actuator is increased to disrupt the mechanisms of flow-induced noise when the amplitude of the detected flow-induced tonal noise is large; and V_{DC} applied to the plasma actuator is reduced to save power consumption when the damping ratio of the shear layer is big and the detected flow-induced tonal noise amplitude is already small. It is worth emphasizing here that the so-called feedback or closed-loop control method used in this work is different from the other classical closed-loop control methods applied to cavity systems [15–19], as the plasma actuator mainly induces spanwise disturbances rather than providing streamwise compensations. Streamwise disturbances are still able to develop due to the interaction between the induced spanwise flows generated by plasma actuators operated in phase across the span of the cavity. It could be studied with a two-dimensional Fourier transform decomposition on the overall three-dimensional flowfield. The detail is beyond the scope of this paper.

A PID controller is easy to develop, simple to tune, robust to disturbance, and has been used extensively. It was developed to demonstrate the closed-loop control scheme using the plasma actuator. The aim here is to use the PID controller to verify the closed-loop control method with the plasma actuator.

Figure 11 shows the structure of the PID controller that was implemented using a dSPACE real-time system. The surface pressure data is passed through a bandpass digital filter to remove the low-frequency wind-tunnel noise and the high-frequency tonal noise of the plasma actuator. The negative feedback signal is then fed into the PID operator, whose coefficients were first tested in MATLAB using the variable structure model and were subsequently tuned manually online. The output PID signal is transferred to a saturation part that prevents possible overflow and underflow. The minimum and maximum limits of the saturation part are 0 and 0.7, respectively, so that a square wave with a duty cycle between 0 and 70% is generated.

Figure 12 shows the instantaneous sound pressure and the corresponding plasma driving signal's duty cycle. The sound pressure signal was measured with the leading-edge microphone and converted by an ADC on the dSPACE real-time system. The duty cycle of the control signal is 0% when the plasma actuator is switched off and it is 70% when the plasma actuator keeps working. The cycle is varied online when the closed-loop control method is applied. The average sound pressure amplitudes are reduced by using both plasma driving signals. When the plasma actuator keeps working, however, it radiates tonal noises with relatively high amplitudes at the harmonic frequencies of the plasma driving signal. An advantage of using the closed-loop control system is that the amplitude of the plasma radiated noise is significantly reduced.

Figure 13 shows the SPL results obtained with the both plasma driving signals at $U_\infty = 15$ m/s. The tonal noises at several Rossiter modes are attenuated when the plasma actuator keeps operating at 20 V and 20 W of system input. There is an approximately 26 dB reduction of the amplitude of the dominant peak. The harmonics of the plasma driving signal at 3.2 kHz, however, are at most 8 dB higher than the attenuated flow-induced tonal noise. In the case of a closed-loop control, the applied input voltage V_{DC} is 30 V to optimize the authority performance of the plasma actuator while the duty cycle of the plasma driving signal is variable online, so the system power consumption is varied, leading to a savings in system power. Compared with Table 2, it can be found that the closed-loop system attenuated the dominant Rossiter mode (the fourth mode) by 16 dB. However, the closed-loop system leads to the amplitude increase at the other Rossiter frequencies (the third and the fifth modes). The mechanism is related to the fundamental limitation of a closed-loop control that can be explained using Bode's integral formula [33]: reducing the sensitivity of a closed-loop system to disturbances at one range of frequencies has to be compromised with worse sensitivity at the other range of frequencies. With the closed-loop method, the maximum radiated plasma noise is reduced by 20 dB. The harmonics of the plasma driving signal at 3.2 kHz are modulated by the closed-loop controller. Their energy is therefore redistributed over a broad frequency range.

Figure 14 shows a comparison of the results obtained with both plasma driving signals at $U_\infty = 20$ m/s. The applied voltage V_{DC} of the plasma actuator using the constant 70% duty cycle was adjusted

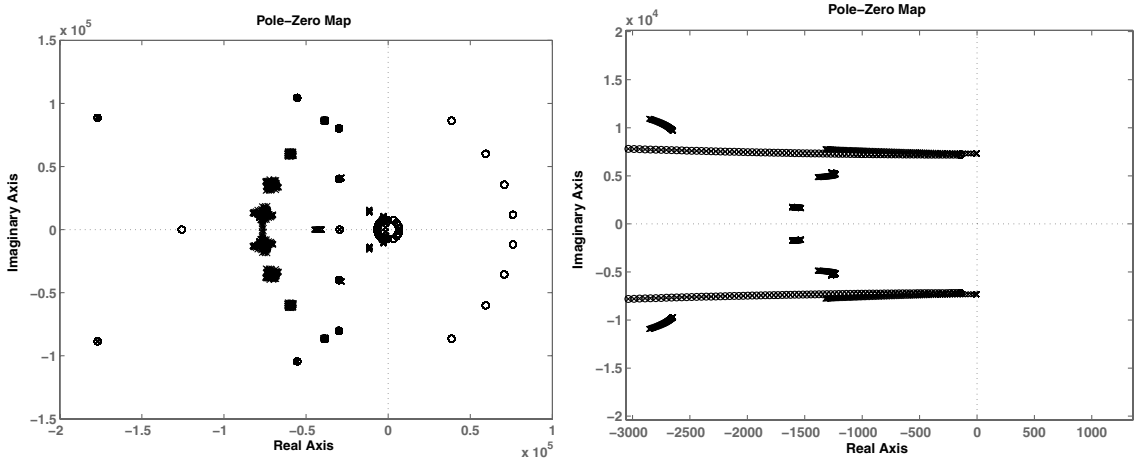

a) The poles-zeros map **b) The enlarged part**

Fig. 10 The poles (x) and zeros (o) of the variable structure model, where $U_\infty = 20$ m/s and the system input voltage of the plasma actuator is from 0 to 30 V.

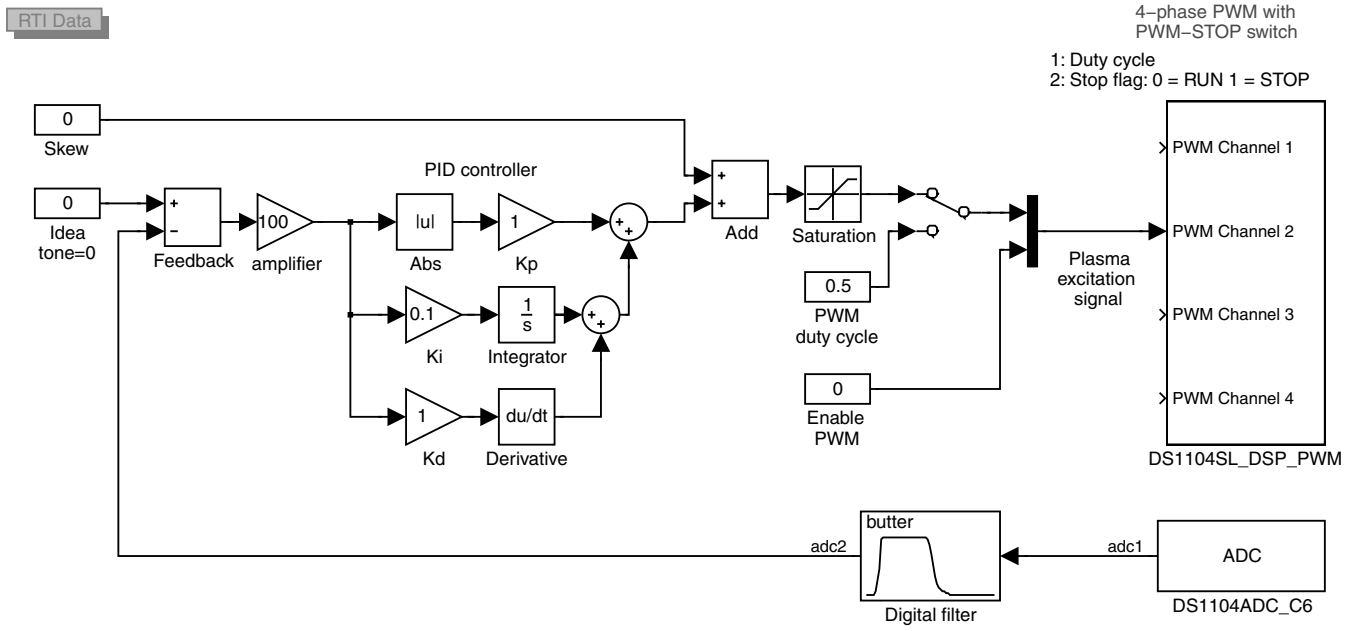

Fig. 11 The implementation of a PID controller using a dSPACE real-time system.

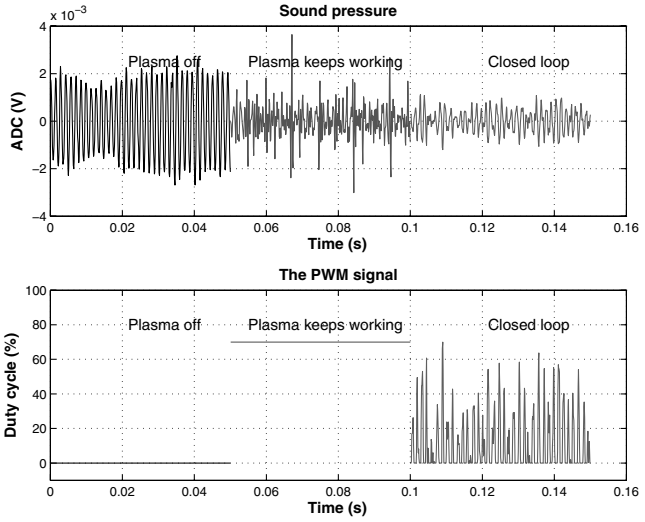

Fig. 12 The measured sound pressure and the corresponding duty cycle of the plasma driving signal at $U_\infty = 15$ m/s.

to achieve the comparable attenuation with the closed-loop control method using the variable duty cycle. In both cases, the energy of the dominant mode (the fifth mode) is redistributed into two Rossiter modes (the fourth and fifth modes) with smaller levels. The plots in Figs. 12 and 14 indicate that the closed-loop control method saves approximately 45% of the system power. The maximum radiated plasma noise is also reduced while its spectrum is redistributed into a broad frequency range and the amplitudes around the harmonics of the plasma driving signal are increased up to 4.5 dB. From the electric point of view, the wider spectrum is caused by the nonperiodical duty cycle. From the control point of view, it can be explained with Bode's integral formula. A more detailed description can be found in Cattafesta et al. [25].

The time-mean flow captured using PIV in the x–z plane slightly below $y = 0$ is shown in Fig. 15, which corresponds to the shear layer region from the leading-edge corner of the cavity to the trailing-edge corner. The employed coordinates are displayed in Fig. 1. The PIV system used in the experiments was produced by Dantec Measurement Systems and incorporates two Gemini Nd:YAG lasers by New Wave Research that are capable of running at 4 Hz and emitting 120 μJ pulses at 532 nm. A Dantec HiSense (type 13 gain 4) 1024 × 1289 resolution charged–coupled device camera was used in

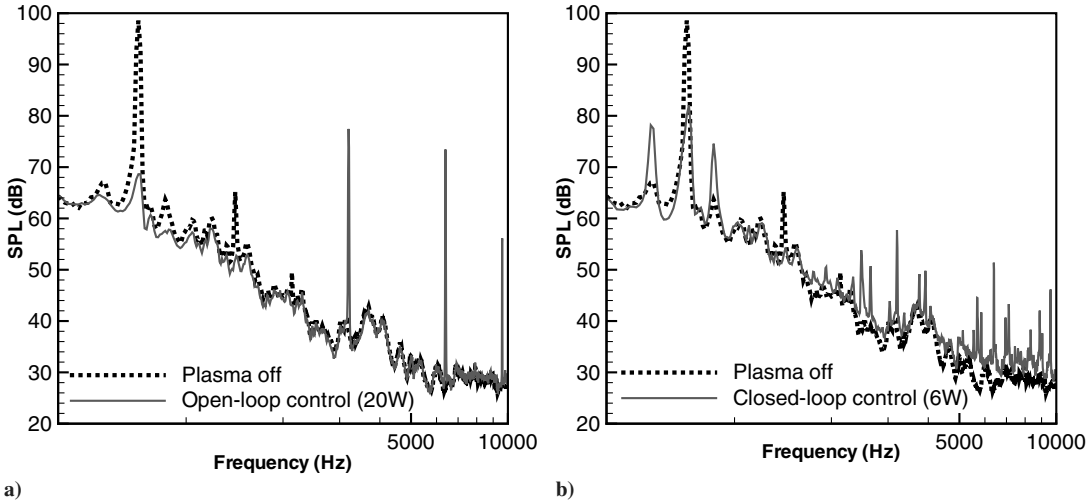

Fig. 13 The attenuated tonal noise with both plasma driving signals at $U_\infty = 15$ m/s: a) the plasma actuator works continuously using 20 W power; and b) the plasma actuator works with the closed-loop control consuming 6 W power.

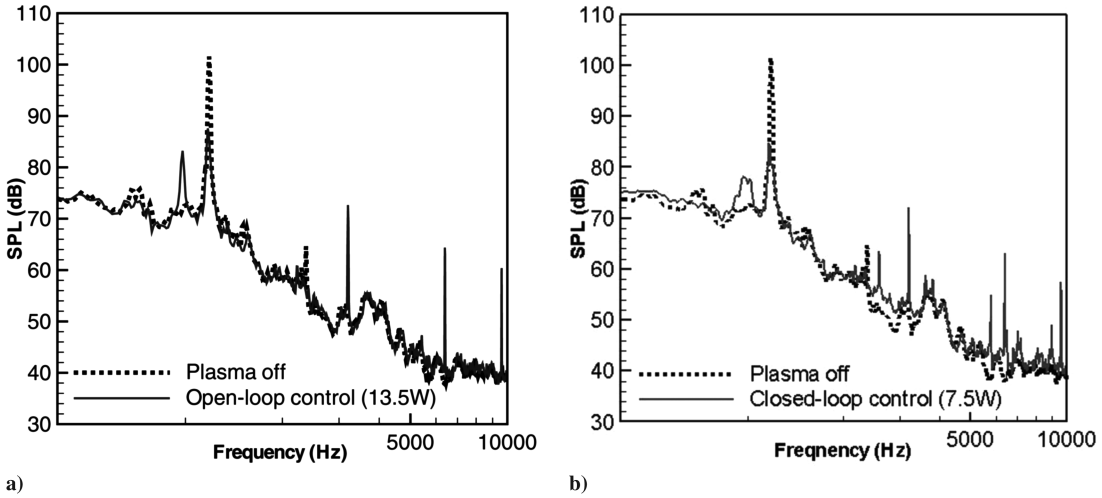

Fig. 14 The attenuated tonal noise with both plasma driving signals at $U_\infty = 20$ m/s: a) the plasma actuator works continuously using 13.5 W power; and b) the plasma actuator works with the closed-loop control consuming 7.5 W power.

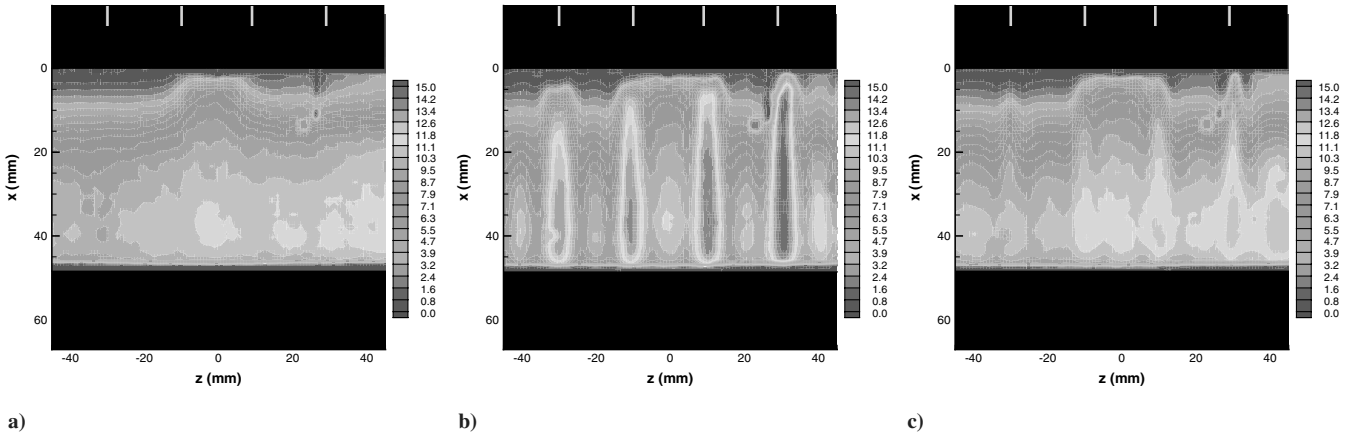

Fig. 15 Contours of the streamwise velocity at $U_\infty = 20$ m/s. The freestream flow is from top to bottom. The plasma actuator operating with: a) 0 V, b) open-loop control at 30 V and 45 W, and c) closed-loop control at 30 V and 7.5 W.

double frame mode for image capture. The lenses available were a Nikon Nikkor 24 mm f/2.8 lens and a Nikon Nikkor 60 mm f/2.8 lens. To provide seeding for the flow, a Safex S195G smoke seeder using regular DJ mix fluid by Martin Professional, Inc. was used. The typical size of the nonspherical particles is 2 μm in diameter. The particles provided suitable tracer material that was homogeneously distributed into the flow. The seeder was placed in the same room as the wind tunnel and care was taken so that the presence of the seeder would not interfere with the flow around the wind tunnel. Image correlations were performed using Dantec's FlowManager to obtain velocity vectors. Typically, image sets were processed using an adaptive correlation with a minimum pixel sized interrogation area of 16×16 with a $75 \times 75\%$ overlap to improve the resolution of the vector map. The processing technique produces a vector map containing up to 317×253 vectors. Inevitably, spurious vectors arise as a result of the finite number of tracer particles in the flow, excessive particle displacements, insufficient resolution, or even poor image quality. The method for removing these spurious vectors is by using a range validation whereby vectors that are greater than a specified magnitude would be rejected. The validation tool is already provided in Dantec's FlowManager.

To produce the time–mean flow, 250 instantaneous vector maps were generated from images collected with a 2 Hz sampling rate. In the figure, the dark regions represent the leading- and trailing-edge surfaces of the cavity; the white strips represent the electrodes of the plasma actuator. Figure 15 shows that both the open-loop and the closed-loop control methods produce a spanwise variation in the streamwise velocity. In Fig. 15b the effect of the plasma actuator on the spanwise flowfield can be clearly seen using the open-loop control method with a 45 W power input. Figure 15c shows that a similar three-dimensional fluid structure is produced using the closed-loop control method with a 7.5 W power input, but the variation is less. In both cases, the observed variation in the flow coincides with the electrode spacing of the plasma actuator, indicating that the upstream disturbances of the plasma actuator convect downstream with the flow and affect the shear layer. Although the three-dimensional variations were observed in both experiments with either the open-loop or the closed-loop method, it is still arguable at the stage whether the fluid dynamics for the noise attenuation is similar. A time-resolved PIV experiment might be helpful to address the problem.

VI. Conclusions

Although there are some open questions for atmospheric air plasma actuators, for example, its sensibility to humidity and air composition under harsh working conditions and the material sustainability to ozone, the fast response (producing glow discharges in nanoseconds) and the simple structure make the actuator a promising option in aerospace control applications. To understand the discharge effect in aeroacoustic applications, we studied the problem of cavity flow-induced tonal noise control. The physics-based linear model was extended to a new variable structure model to describe the dynamics of the system using the plasma actuator. The study showed that the predictions of the dominant peak matched the measured data well at $U_\infty = 20$ m/s when a linear relationship

between the applied system voltage and the damping ratio of the second-order shear layer model was assumed. The good agreements were also obtained for other cases at the lower investigated velocities. As a result, the plasma actuator was regarded as a linear gain and the overall cavity system was described with the variable structure model, which would improve the understanding of the plasma actuator working effect for low-speed flow-induced noise attenuation from a control perspective. The effect at the higher velocities, however, is not studied yet.

To demonstrate the closed-loop control system with the plasma actuator, a PID controller was implemented using the dSPACE real-time system. The control parameters were tested by MATLAB using the variable structure model and tuned manually online. Compared with the method in which the plasma actuator kept working, the PID method improved the power efficiency by at least 45%. It proved the advantage of a closed-loop control method. However, the effectiveness of the PID method in attenuating the dominant Rossiter mode was less than that achieved by the open-loop system. To exploit the full potential of the control schemes and to design a more effective system, more advanced control strategies such as the design method of a linear quadratic regulator could be considered.

Acknowledgments

The majority of this research was done while Xun Huang and Sammie Chan were Ph.D. students and supported by studentships from the School of Engineering Sciences, University of Southampton, United Kingdom.

References

[1] Roth, J. R., Sherman, D. M., and Wilkinson, S. P., "Electrohydrodynamic Flow Control with a Glow-Discharge Surface Plasma,"*AIAA Journal*, Vol. 38, No. 7, July 2000, pp. 1166–1172.

[2] Roth, J. R., Sin, H., Mohan, R. C. M., and Wilkinson, S. P., "Re-Attachment and Acceleration by Paraelectric and Peristaltic Electrohydrodynamic Effects," AIAA Paper 2003-0531, 2003.

[3] Roth, J. R., "Aerodynamic Flow Acceleration Using Paraelectric and Peristaltic Electrohydrodynamic Effects of a One Atmosphere Uniform Glow Discharge Plasma (OAUGDP)," *Physics of Plasmas*, Vol. 10, No. 5, 2003, pp. 2117–2126. doi:10.1063/1.1564823

[4] Roth, J. R., Sherman, D. M., and Wilkinson, S. P., "Boundary Layer Flow Control with a One Atmosphere Uniform Glow Discharge Surface Plasma," AIAA Paper 1998-0328, 1998.

[5] Roth, J. R., "Electrohydrodynamically Induced Airflow in a One Atmosphere Uniform Glow Discharge Surface Plasma," *25th IEEE International Conference on Plasma Science*, No. 6P-67, IEEE Publications, Piscataway, NJ, June 1998.

[6] Enloe, C. L., McLaughlin, T. E., Van Dyken, R. D., Kachner, K. D., Jumper, E. J., Corke, T. C., Post, M., and Haddad, O., "Mechanisms and Responses of a Dielectric Barrier Plasma Actuator: Geometric Effects," *AIAA Journal*, Vol. 42, No. 3, 2004, pp. 595–604.

[7] Enloe, C. L., McLaughlin, T. E., Van Dyken, R. D., Kachner, K. D., Jumper, E. J., and Corke, T. C., "Mechanisms and Responses of a Single Dielectric Barrier Plasma Actuator: Plasma Morphology," *AIAA Journal*, Vol. 42, No. 3, 2004, pp. 589–594.

[8] Corke, T., He, C., and Patel, M., "Plasma Flaps and Plasma Slats: An Application of Weakly-Ionized Plasma Actuators," AIAA Paper 2004-2127, 2004.

[9] Moreau, E., "Airflow Control by Non-Thermal Plasma Actuators," *Journal of Physics D: Applied Physics*, Vol. 40, No. 3, 2007, pp. 605–636. doi:10.1088/0022-3727/40/3/S01

[10] Santhanakrishnan, A., and Jacob, J. D., "Flow Control with Plasma Synthetic Jet Actuators," *Journal of Physics D: Applied Physics*, Vol. 40, No. 3, 2007, pp. 637–651. doi:10.1088/0022-3727/40/3/S02

[11] Labergue, A., Moreau, E., Zouzou, N., and Touchard, G., "Separation Control Using Plasma Actuators: Application to a Free Turbulent Jet," *Journal of Physics D: Applied Physics*, Vol. 40, No. 3, 2007, pp. 674–684. doi:10.1088/0022-3727/40/3/S05

[12] Thomas, O. F., Kozlov, A., and Corke, C. T., "Plasma Actuators for Landing Gear Noise Reduction," AIAA Paper 2005-3010, 2005.

[13] Chan, S., Zhang, X., and Gabriel, S., "The Attenuation of Cavity Tones Using Plasma Actuators," *AIAA Journal*, Vol. 45, No. 7, 2007, pp. 1525–1538. doi:10.2514/1.26645

[14] Huang, X., Chan, S., and Zhang, X., "An Atmospheric Plasma Actuator for Aeroacoustic Applications," *IEEE Transactions on Plasma Science*, Vol. 35, No. 3, 2007, pp. 693–695. doi:10.1109/TPS.2007.896781

[15] Cabell, R. H., Kegerise, M. A., Cox, D. E., and Gibbs, G. P., "Experimental Feedback Control of Flow-Induced Cavity Tones," *AIAA Journal*, Vol. 44, No. 8, Aug. 2006, pp. 1807–1815. doi:10.2514/1.19608

[16] Yan, P., Debiasi, M., Yuan, X., Little, J., Ozbay, H., and Samimy, M., "Experimental Study of Linear Closed-Loop Control of Subsonic Cavity Flow," *AIAA Journal*, Vol. 44, No. 5, May 2006, pp. 929–938.

[17] Cattafesta, L. N., Garg, S., Choudhari, M., and Li, F., "Active Control of Flow-Induced Cavity Resonance," AIAA Paper 1997-1084, 1997.

[18] Cattafesta, L. N., Shukla, D., Garg, S., and Ross, J. A., "Development of an Adaptive Weapons-Bay Suppression System," AIAA Paper 1999-1901, 1999.

[19] Rowley, C. W., Williams, D. R., Colonius, T., Murray, R. M., and MacMynowski, D. G., "Linear Models for Control of Cavity Flow Oscillations," *Journal of Fluid Mechanics*, Vol. 547, 2006, pp. 317–330. doi:10.1017/S0022112005007299

[20] Samimy, M., Debiasi, M., Caraballo, E., Serrani, A., Yuan, X., Little, J., and Myatt, J. H., "Feedback Control of Subsonic Cavity Flows Using Reduced-Order Models," *Journal of Fluid Mechanics*, Vol. 579, 2007, pp. 315–346. doi:10.1017/S0022112007005204

[21] Williams, D. R., and Rowley, C. W., "Recent Progress in Closed-Loop Control of Cavity Tones," AIAA Paper 2006-0712, 2006.

[22] Rowley, C. W., and Williams, D. R., "Dynamics and Control of High-Reynolds-Number Flow over Open Cavities," *Annual Review of Fluid Mechanics*, Vol. 38, 2006, pp. 251–276. doi:10.1146/annurev.fluid.38.050304.092057

[23] Roth, J. R., *Industrial Plasma Engineering: Applications to Nonthermal Plasma Processing*, Vol. 2, Inst. of Physics Publishing, London, 2001, Chap. 18.

[24] Pons, J., Moreau, E., and Touchard, G., "Asymmetric Surface Dielectric Barrier Discharge in Air at Atmospheric Pressure: Electrical Properties and Induced Airflow Characteristics," *Journal of Physics D: Applied Physics*, Vol. 38, No. 19, 2005, pp. 3635–3642. doi:10.1088/0022-3727/38/19/012

[25] Cattafesta, L. N., Williams, D., Rowley, C., and Alvi, F., "Review of Active Control of Flow-Induced Cavity Resonance," AIAA Paper 2003-3567, 2003.

[26] Kegerise, M. A., Cabell, R. H., and Cattafesta, L. N., "Real-Time Adaptive Control of Flow-Induced Cavity Tones," AIAA Paper 2004-0572, 2004.

[27] Culick, F. E. C., *Dynamics of Combustion Systems: Fundamentals, Acoustics, and Control II. Principles and Methods of Classical Control in the Frequency Domain*, A Short Course of Lectures from California Inst. of Technology, California Inst. of Technology, 2001.

[28] Rossiter, J. E., "Wind-Tunnel Experiments on the Flow over Rectangular Cavities at Subsonic and Transonic Speeds," Aeronautical Research Council Report Memo 3438, 1964.

[29] Font Gabriel, I., "Boundary-Layer Control with Atmospheric Plasma Discharges," *AIAA Journal*, Vol. 44, No. 7, July 2006, pp. 1572–1578.

[30] Shyy, W., Jayaraman, B., and Andersson, A., "Modeling of Glow Discharge-Induced Fluid Dynamics," *Journal of Applied Physics*, Vol. 92, No. 11, Dec. 2002, pp. 6434–6443. doi:10.1063/1.1515103

[31] Chen, Z. Y., "PSPICE Simulation of One Atmosphere Uniform Glow Discharge Plasma (OAUGDP) Reactor Systems," *IEEE Transactions on Plasma Science*, Vol. 31, No. 4, 2003, pp. 511–520. doi:10.1109/TPS.2003.815241

[32] Baker, G. A., Jr. and Graves-Morris, *Padé Approximants*, Cambridge Univ. Press, New York, 1996.

[33] Bode, H. W., *Network Analysis and Feedback Amplifier Design*, D. Van Nostrand Company, Inc., Princeton, NJ, 1945.

D. Gaitonde
Associate Editor